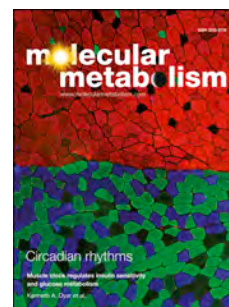# Journal Pre-proof

Truncation of Pik3r1 causes severe insulin resistance uncoupled from obesity and dyslipidemia by increased energy expenditure

Albert Kwok, Ilona Zvetkova, Sam Virtue, Ineke Luijten, Isabel Huang-Doran, Patsy Tomlinson, David A. Bulger, James West, Steven Murfitt, Julian Griffin, Rafeah Alam, Daniel Hart, Rachel Knox, Peter Voshol, Antonio Vidal-Puig, Jørgen Jensen, Stephen O'Rahilly, Robert K. Semple

Please cite this article as: Kwok A, Zvetkova I, Virtue S, Luijten I, Huang-Doran I, Tomlinson P, Bulger DA, West J, Murfitt S, Griffin J, Alam R, Hart D, Knox R, Voshol P, Vidal-Puig A, Jensen J, O'Rahilly S, Semple RK, Truncation of Pik3r1 causes severe insulin resistance uncoupled from obesity and dyslipidemia by increased energy expenditure, *Molecular Metabolism*, https://doi.org/10.1016/j.molmet.2020.101020.

1
2
Truncation of Pik3r1 causes severe insulin resistance uncoupled from obesity and dyslipidemia by increased energy expenditure

3

4
SHORT TITLE: Insulin resistance without lipotoxicity due to Pik3r1 mutation

5

6
Albert Kwok[1,2], Ilona Zvetkova[1,2], Sam Virtue[1,2], Ineke Luijten[3], Isabel Huang-

7
Doran[1,2], Patsy Tomlinson[1,2], David A. Bulger[1,2], James West[4], Steven Murfitt[4], Julian

8
Griffin[4,8], Rafeah Alam[5], Daniel Hart[1,2], Rachel Knox[1,2], Peter Voshol[6], Antonio Vidal-

9
Puig[1,2], Jørgen Jensen[7], Stephen O'Rahilly[1,2], Robert K Semple[3,1,2]

10
11 [1]The University of Cambridge Metabolic Research Laboratories, Wellcome Trust-MRC
12 Institute of Metabolic Science, Cambridge, UK
13 [2]MRC Metabolic Diseases Unit, Wellcome Trust-MRC Institute of Metabolic Science,
14 Cambridge, UK
15 [3]Centre for Cardiovascular Science, University of Edinburgh, 47 Little France Crescent,
16 Edinburgh, UK
17 [4]Department of Biochemistry and Cambridge Systems Biology Centre, University of
18 Cambridge, Cambridge, UK
19 [5]Laboratory of Lymphocyte Signalling and Development, The Babraham Institute,
20 Cambridge, UK
21 [6]Louis Bolk Institute, Kosterijland 3-5, NL-3981AJ, Bunnik, The Netherlands
22 [7]Department of Physical Performance, Norwegian School of Sport Sciences, P.O. Box 4014,
23 Ulleval Stadion, 0806 Oslo, Norway
24 [8]Biomolecular Medicine, Division of Systems Medicine, Department of Metabolism, Digestion
25 and Reproduction, Medicine, Imperial College London, The Sir Alexander Fleming Building,
26 London, UK
27

28 **Correspondence to:**
29 Prof. Robert K. Semple, Centre for Cardiovascular Science, University of Edinburgh,
30 Queen's Medical Research Institute, Little France Crescent, Edinburgh EH16 4TJ,
31 UK. Tel: +44 131 242 6051/ Email: rsemple@ed.ac.uk
32
33

1   **SUMMARY**[1]

2   Objective: Insulin signaling via phosphoinositide 3-kinase (PI3K) requires *PIK3R1*-

3   encoded regulatory subunits.   C-terminal *PIK3R1* mutations cause SHORT

4   syndrome, including lipodystrophy and insulin resistance (IR), surprisingly without

5   fatty liver or metabolic dyslipidemia. We sought to investigate this discordance.

6   Methods: The human pathogenic *Pik3r1* Y657* mutation was knocked into mice by

7   homologous recombination. Growth, body composition, bioenergetic and metabolic

8   profiles were investigated on chow and high fat diet. Adipose and liver histology was

9   examined, and liver responses to fasting and refeeding assessed transcriptomically.

10   Results: Like humans with SHORT syndrome, *Pik3r1*$^{Y657*/WT}$ mice were small with

11   severe IR, and adipose expansion on high fat diet was markedly reduced. Also like

12   humans, plasma lipid concentrations were low, and insulin-stimulated hepatic

13   lipogenesis was not increased despite hyperinsulinemia. At odds with lipodystrophy,

14   however, no adipocyte hypertrophy nor adipose inflammation was found. Liver

15   lipogenic gene expression was not significantly altered, and unbiased

16   transcriptomics showed only minor changes, including evidence of reduced

17   endoplasmic reticulum stress in the fed state and diminished Rictor-dependent

18   transcription on fasting. Increased energy expenditure, which was not explained by

19   hyperglycemia nor intestinal malabsorption, provided an alternative explanation for

20   uncoupling of IR from dyslipidaemia.

21   Conclusions: *Pik3r1* dysfunction in mice phenocopies the IR and reduced adiposity

22   without lipotoxicity of human SHORT syndrome. Decreased adiposity may not reflect

23   *bona fide* lipodystrophy, but rather increased energy expenditure, and we suggest

24   that study of brown adipose tissue in both humans and mice is warranted.

25

26   **Keywords**: Insulin resistance, diabetes, lipotoxicity, PI 3-Kinase, p85, Pik3r1, lipids
27

---

[1] Abbreviations: IR = insulin resistance; PI3K = phosphoinositide 3-kinase; SHORT syndrome = Short stature, Hyperextensibility of joints, Ocular depression, Rieger anomaly of the iris, and Teething delay; RER = Respiratory Exchange Ratio; HFD = High Fat Diet

1   **1. Introduction**

2   Adipose tissue is essential for metabolic health in the face of sustained positive

3   energy. When adipose expansion is constrained, as in lipodystrophy, its capacity to

4   sequester excess energy and serve as a physiological "energy buffer" is

5   overwhelmed [1]. Injury and inflammation of any residual adipose tissue ensues,

6   causing systemic inflammation and rerouting substrates to liver, pancreas and

7   muscle. Insulin resistance (IR), diabetes, aggressive fatty liver disease, and

8   severely elevated plasma lipoprotein concentrations are thus common

9   consequences of lipodystrophy [2].

10   SHORT syndrome (short stature, hyperextensibility of joints, ocular

11   depression, Rieger anomaly of the iris, and teething delay) is a human monogenic

12   syndrome including lipodystrophy [3–5]. This form of lipodystrophy is highly unusual,

13   as although associated with insulin resistant diabetes [3–5], it is uncoupled from fatty

14   liver and dyslipidemia [6]. SHORT syndrome also does not feature the suppressed

15   plasma adiponectin concentration seen in common IR and other lipodystrophies [7],

16   showing that "insulin resistance syndrome" components are dissociable.

17   SHORT syndrome is caused by mutations in *PIK3R1*, encoding components of

18   the insulin signaling enzyme phosphoinositide 3-kinase (PI3K) [3–5]. The PI3K

19   subtype required for insulin action comprises a p110α catalytic subunit bound to a

20   regulatory subunit, three of which - p85α, p55α and p50α – are encoded by *PIK3R1*.

21   *PIK3R1* products stabilise catalytic subunits, mediating their recruitment to receptor

22   tyrosine kinases or their substrates, including the insulin receptor and IRS1 [8,9].

23   Before discovery of *PIK3R1* mutations in SHORT syndrome, *Pik3r1* had been

24   intensively studied in mice. Selective p85α deficiency [10][11] or deletion of p50α

25   and p55α [12] surprisingly enhances insulin sensitivity, which has been accounted

26   for by compensation by other regulatory subunits, and/or altered stoichiometry of

27   catalytic and regulatory subunits. A critical insight from study of SHORT syndrome

1   was that the insulin signaling role of PIK3R1 could be severely attenuated by

2   neomorphic mutations disrupting the C terminal SH2 domain [3–5]. Such dominant

3   negative PIK3R1 alleles, which severely reduce insulin-induced activation of PI3K

4   without abolishing expression of PI3K, offer the opportunity to interrogate *in vivo*

5   pathophysiological roles of PI3K activity in IR more precisely than possible to date.

6   In human lipodystrophy, *de novo* lipogenesis contributes significantly to liver

7   triglyceride and plasma lipid content [13]. In contrast, mutations in the *INSR* gene,

8   encoding the insulin receptor, produce extreme IR with normal plasma lipid profile,

9   normal liver lipid content, and no increase in hepatic *de novo* lipogenesis [13].

10   Furthermore murine models with knockout of any one of several components of the

11   insulin signaling pathway (*Insr* [14], *Irs1* and *Irs2* [15], p85α and β [16], *Pik3ca* [17],

12   or *Rictor* [18]) demonstrate that liver insulin signaling drives hepatic *de novo*

13   lipogenesis. We thus hypothesised that in SHORT syndrome the liver is protected

14   from increased insulin-mediated lipogenesis, which is relatively unaffected by

15   common IR [19], and that this explains the absence of dyslipidemia and fatty liver

16   despite severe IR and lipodystrophy.

17   We report a novel murine SHORT syndrome model caused by a human

18   pathogenic allele, Y657*, that reproduces uncoupling of metabolic dyslipidemia from

19   severe IR. Surprisingly hepatic lipogenic transcriptional programmes were minimally

20   perturbed, although metabolic inflexibility with a dyscoordinated fasting response

21   was seen. Adipose tissue accumulation was reduced on high fat feeding. We

22   suggest that this is related to increased energy expenditure, likely via brown adipose

23   tissue, rather than lipodystrophy, with hypolipidemia attributable to increased fuel

24   oxidation. This potential explanation for the unusual IR subphenotype of SHORT

25   syndrome warrants testing in humans with SHORT syndrome or other defects in

26   proximal insulin signaling.

27

28   **2. Materials and Methods**

1 **2.1 Mice generation and maintenance**

2 The *Pik3r1* Y657* mutation and a neomycin resistance cassette flanked by

3 LoxP sites were introduced into C57Bl/6 embryonic stem cells by homologous

4 recombination before injection into Bl/6J blastocysts (**Supplemental Figure S1**).

5 Animals were kept on a C57Bl/6J background, backcrossed at least three times, and

6 housed on a 12-hour-light/12-hour-dark cycle at 23°C, with *ad libitum* food and water

7 access. Feeding was with chow (Catalogue no. 105, Safe diets) or 45% fat diet (45%

8 fat, 35% Carbohydrate and 25% protein) (Catalogue no. D12451, Research diet,

9 Inc). Experiments were carried out under the UK Home Office Animals (Scientific

10 Procedures) Act 1986, following University of Cambridge ethical review.

11 **2.2 Assessment of growth, body composition, and energy homeostasis**

12 Body composition was determined by time-domain NMR with Bruker's

13 minispec analyser. For food intake and energy expenditure measurement, male mice

14 were acclimatized for 1 week to single housing then given chow or 45% fat diet for

15 10 days. Food intake was measured daily and energy expenditure measured by

16 indirect calorimetry [20]. Locomotor activity was quantified as beam breaks over 48

17 hours. Fecal energy content was measured by combusting dried feces from 48hr

18 calorimeter runs in an IKA Calorimeters Oxygen Bomb calorimeter (IKA C1).

19 **2.3 *In vivo* metabolic studies**

20 For fasting/refeeding studies, mice were fed chow *ad libitum* until 16 weeks

21 before 16 hours fasting then 6 hours refeeding with chow. Tissues were harvested

22 and snap frozen prior to overnight fasting, or after fasting or after refeeding. For

23 study of insulin action 16 hour-fasted mice (16 weeks old) were injected with 2U/kg

24 insulin intraperitoneally and tissues collected after 10 minutes and snap frozen.

25 Glucose tolerance testing was undertaken on overnight (16 hour) fasted mice using

26 2g/kg 20% glucose *via* oral gavage. For insulin tolerance testing 6 hour-fasted mice

27 were given 0.5U/kg intraperitoneal insulin. For lipid tolerance testing 16 hour-fasted

28 mice were administered 10mL/kg olive oil by gavage.

1   Hyperinsulinemic euglycemic clamp studies and subsequent sample

2   processing and analysis were conducted as described previously [21] on 16 week

3   old mice after overnight fasting. Clamps used a priming dose of human insulin (0.7

4   mU), followed by constant insulin and [3-^{3}H]-D-glucose infusion at 7 mU/h and 0.72

5   µCi/h, respectively.

6   **2.4 Study of tissue insulin responsiveness *ex vivo***

7   Measurement of insulin action on isolated Soleus and Extensor Digitorum

8   Longus was undertaken in 16 week old male mice as described[22]. For primary

9   preadipocyte differentiation studies fat pads from 8 week-old male mice were

10   isolated and cultured as described [20], but without 5-Triiodo-l-thyronine.

11   **2.5 Biochemical assays**

12   Blood was collected by cardiac puncture and plasma snap frozen before

13   assays detailed in supplemental Table 3. Glycogen content of snap-frozen liver used

14   glycogen hydrolysis in 1 M HCl (2.5 h at 100°C), NaOH neutralization and

15   fluorometric glucose analysis [23]. Hepatic triglyceride determination used a

16   Triglyceride Colorimetric Assay kit (Cayman). Hepatic cholesterol was extracted from

17   10mg liver using 400uL chloroform:isopropanol:NP-40 mixture (7:11:0.1) before

18   centrifugation, 30min vacuum drying (50°C) and dissolving in PBS. The samples

19   were assayed by Siemens Healthcare Diagnostics kit.

20   **2.6 Metabolomic Studies**

21   Liver metabolites were extracted from tissue snap-frozen after dissection using

22   a reported methanol/chloroform method [24]. Aqueous metabolites were further

23   extracted as described in [24] and analysed using a Vanquish ultra-high

24   performance liquid chromatography (UHPLC) system and TSQ Quantiva triple

25   quadrupole mass spectrometer (Thermo Scientific) with compounds directly infused.

26   Parameter optimisation used 1µM standard solutions in chromatographic buffer.

27   Optimal mass spectrometry parameters and mass transitions were generated by

1 automatic MassLynx™ (Version 1.4, Waters) protocols or, if standards were

2 unavailable, deduced from known analogue parameters.

2.7 Assessment of *de novo* lipogenesis

4 16 week chow-fed mice were fasted overnight, injected intraperitoneally with

5 deuterated saline (24 uL/g), and given high carbohydrate diet (Harlan Teklad Diets,

6 Cat no. TD88232) and 4% deuterated water (Goss Scientific Instruments Ltd, Cat

7 no. DLM-2259) from 1- 24 hours later. After culling livers were snap-frozen and

8 50mg homogenised in 600uL methanol-chloroform (2:1) before extraction and

9 analysis as described [25].

2.8 Histology

11 Size of at least 1000 adipocytes per genotype from 16 week old chow-fed mice was

12 measured in FFPE tissue as described [26]. Adipose Treg cells were isolated and

13 counted by FACS, also as reported [27].

2.9 Gene expression analysis

15 For protein studies fresh tissues were snap-frozen in liquid nitrogen, and

16 homogenised using MD ceramic beads in RIPA buffer with proteinase/phosphatase

17 inhibitors (liver, muscle)(Roche) or mortar and pestle in liquid nitrogen before

18 dissolving in buffer (adipose). Protein concentrations were determined by BCA assay

19 (BioRad). Western blotting employed the Novex gel system (Thermo Fisher

20 Scientific). Antibodies are shown in Supplemental Table S4.   Quantification

21 employed the BioRad image system.

22 Total RNA was extracted and reverse transcribed for qPCR as previously

23 described [28]. Target expression was normalised to the geometric mean of 4

24 housekeeping genes (Ywhaz, Ppia, B2m and Eef1a1) (Supplemental Table S4 for

25 primer/probe sequences). RNA sequencing protocols and analysis have previously

26 been reported [29].

2.10 Statistical Analysis

1   D'Agostino & Pearson or Shapiro-Wilk tests were performed to test for

2   Gaussian distribution of data. For Gaussian data unpaired two-tailed Student's t

3   tests for two group comparison and ANOVA with *post hoc* for multiple group

4   comparison were performed using GraphPad Prism (GraphPad Software). For non

5   Gaussian data Mann-Whitney testing was used for two group comparison and

6   Kruskal-Wallis and Dunn's multiple comparison testing were used for multiple group

7   analysis using GraphPad Prism (GraphPad Software). Tissue weights, food

8   consumption and energy expenditure were analyzed by ANCOVA using XLSTAT

9   (Addinsoft).

10   **2.11 Data and Resource Availability**

11   All transcriptomic data were deposited in GEO under accession number XXXX

12   (http://www.ncbi.nlm.nih.gov/geo/query/acc.cgi?acc=XXXX).   Other datasets, and

13   the *Pik3r1*$^{Y657*/WT}$ mice generated during the current study are available from the

14   corresponding author upon reasonable request.

15

16   **3. Results**

17   **3.1 Growth and development of Pik3r1 Y657* knock-in mice**

18   Mice harbouring the *Pik3r1* Y657* mutation were generated by homologous

19   recombination-based gene targeting (**Figure S1A**).   Immunoblotting confirmed

20   expression of truncated p85α at greater amounts than full length protein in most

21   tissues, likely due to loss of a ubiquitylation motif located beyond the nonsense

22   mutation in the C-terminal [30]. No compensatory change in PI3K p85β subunit was

23   seen. p110α subunit expression was reduced in subcutaneous white adipose tissue,

24   and p110β expression was reduced in liver, subcutaneous and epididymal white

25   adipose tissue (**Figure S1B**).

26   No *Pik3r1*$^{Y657*/Y657*}$ embryos were identified beyond E11.5. At E11.5 they were

27   smaller, with poorly developed limb buds and reduced eye pigmentation.

1 Heterozygous embryos were smaller from E15.5 (**Figure S2A-E**).   *Pik3r1$^{WT/Y657*}$*

2 mice were born at expected frequency but showed impaired linear growth and body

3 weight on chow (**Figure 1A-C**). At 16 weeks there was a small decrease in whole

4 body adiposity (**Figure 1D**), however no difference was found in epididymal or

5 inguinal white adipose nor interscapular brown adipose depot weights when lean

6 mass was taken into account (**Figure 1E-G**).   Plasma leptin concentrations were

7 similar in male *Pik3r1$^{WT/Y657*}$* and wild-type mice (3.3±1.2 *vs* 2.6±0.3 μg/L on fasting

8 (n=9,10; NS); 10.3±2.2 *vs* 15.9±3.9 μg/L on *ad libitum* feeding (n=13,13; NS)). Liver

9 weights were indistinguishable (**Figure 1H**), but hearts were heavier in *Pik3r1$^{WT/Y657*}$*

10 mice (**Figure 1I**). No difference in food consumption nor energy expenditure was

11 seen at 16 weeks on chow (**Figure 1J,K**), however the respiratory exchange ratio

12 (RER) was higher during the light phase in *Pik3r1$^{WT/Y657*}$* mice, blunting circadian

13 fluctuation (**Figure 1L**). Similar differences were seen between heterozygous and

14 wild-type females for all variables assessed in both sexes.

15 **3.2 Response of *Pik3r1$^{WT/Y657*}$* mice to a high fat diet**

16   To assess whether placing a greater load on adipose tissue in *Pik3r1$^{WT/Y657*}$*

17 mice would unmask lipodystrophy, mice were fed a 45% fat diet (HFD) from 8 weeks

18 old. *Pik3r1$^{WT/Y657*}$* mice showed reduced gain of weight and body fat over the 8

19 weeks studied (**Figure 2A,B**).   Epididymal white adipose tissue was most severely

20 affected (**Figure 2C**), with no significant difference in inguinal nor brown adipose

21 tissue (**Figure 2D,E**).   Lean mass did not increase at a greater rate in *Pik3r1$^{WT/Y657*}$*

22 mice (**Figure S3A,B**), and liver weights also did not differ, while heart weights were

23 elevated in heterozygotes, as on chow (**Figure 2F,G**).   Consistent with reduced

24 adiposity, *Pik3r1$^{WT/Y657*}$* mice had lower serum leptin concentration when fed

25 (37.7±7.3 *vs* 11.3±2.0 μg/L (n=15,11; p=3x10^{-3})), but not fasted (15.9±3.9 *vs*

26 10.3±2.2 μg/L (n=13,13; not significant)), while adiponectin concentrations were

27 unchanged (**Table 1**).

9

1   Given reduced adipose expansion, we next sought histological evidence of

2   "adipose failure", namely adipocyte hypertrophy and inflammation, which would be

3   expected in lipodystrophy when adipose expansion is pathological constrained,

4   causing adipose injury on positive energy balance. The histological appearance and

5   adipocyte size distribution in epididymal adipose tissue was indistinguishable

6   between genotypes (**Figure 2H,I**), however, with no evidence of inflammation, nor

7   fibrosis. Consistent with the lack of histological evidence of adipose overload, *ex*

8   *vivo* differentiation of preadipocytes from inguinal or epididymal depots was

9   unaltered (**Figure 2J**). Finally, given the role of *Pik3r1* in lymphocyte function, and

10   the important role of adipose-resident T regulatory (T_{reg}) cells in energy homeostasis,

11   the adipose content of T_{reg} cells was assessed by FACS. No major difference was

12   observed between genotypes (**Figure 2K**).

13   Given these findings, which are at odds with a true lipodystrophy, we next

14   assessed whether reduced adipose accretion instead reflected altered energy

15   homeostasis. *Pik3r1$^{WT/Y657*}$* mice exhibited increased food intake (**Figure 2L**) and

16   energy expenditure (**Figure 2M**) when the size of the animals was taken into

17   account, but locomotor activity was unchanged across 24 hours (**Figure 2N**).

18   Markedly reduced accumulation of adipose tissue despite increased food intake, and

19   without sustained hyperglycemia, demonstrates severely reduced food efficiency.

20   This indicates that increased food intake is a compensatory response to chronically

21   increased energy expenditure rather than a primary phenomenon. As on chow, the

22   circadian RER profile was blunted, with higher values in the dark phase and no

23   discernible difference between light and dark phases for *Pik3r1$^{WT/Y657*}$* mice (**Figure**

24   **2O**), suggesting greater carbohydrate oxidation in the dark phase.

25   **3.3 *Pik3r1$^{WT/Y657*}$* mice are severely insulin resistant**

26   At 12 weeks old, neither male nor female *Pik3r1$^{WT/Y657*}$* mice on chow were

27   hyperglycemic compared to controls, but plasma insulin concentrations were raised,

28   more severely on feeding (**Tables 1** and **S1**). On high fat feeding male *Pik3r1$^{WT/Y657*}$*

1   mice remained hyperinsulinemic, but the difference between mutant and control

2   mice was abolished by the greater increase in insulin concentrations in wild-type

3   mice. Blood glucose concentration was paradoxically lower in fed $Pik3r1^{WT/Y657*}$ mice

4   on high fat diet. Plasma adiponectin concentrations in fasted chow-fed $Pik3r1^{WT/Y657*}$

5   mice were lower than in wild-type controls, however no significant difference was

6   seen in other conditions despite the severe IR of heterozygous mice (**Table 1**). In

7    $Pik3r1^{WT/Y657*}$ mice on HFD, adiponectin normalised to body fat was higher than in

8   controls, reminiscent of the preserved adiponectin seen in severely insulin resistant

9   patients with SHORT syndrome [7]. Normalised plasma leptin concentrations, in

10   contrast, were lower (**Figure S3C,D**).

11   Hyperinsulinemic euglycemic clamps were undertaken on chow- and HFD-fed

12   male mice. Chow-fed $Pik3r1^{WT/Y657*}$ mice required a steady state glucose infusion

13   rate of only one eighth that required by wild-type mice, confirming severe IR (**Figure**

14   **3A**). On HFD $Pik3r1^{WT/Y657*}$ mice remained extremely insulin resistant, however the

15   difference between genotypes was much smaller than on chow due to increased IR

16   in wild-type animals (**Figure 3A**). Further studies were thus undertaken on chow.

17   Glucose and insulin excursions on oral glucose tolerance testing showed a trend

18   towards an increase in male $Pik3r1^{WT/Y657*}$ mice (**Figure 3B,C**), but were increased in

19   female mice (**Figure S4A,B)**, while the hypoglycemic response to insulin was

20   attenuated in both sexes (**Figures 3D** and **S4C**). Clamp studies in males using

21   isotopic tracers showed glucose disposal to be 19% lower in $Pik3r1^{WT/Y657*}$ mice

22   (**Figure 3E**) while suppression of hepatic glucose production by hyperinsulinemia

23   was 49% lower compared to wild type littermates (**Figure 3F**). Despite this, liver

24   glycogen content was similar between genotypes (**Figure 3G**). Insulin infusion

25   lowered plasma free fatty acid concentration in wild-type mice, but little suppression

26   was seen in heterozygous mice, consistent with impaired suppression of adipose

27   lipolysis (**Figure 3H**).

1   Intraperitoneal insulin in male mice strongly induced Akt phosphorylation in

2   liver, skeletal muscle and epididymal and inguinal adipose tissue of wild-type

3   controls, as expected, and this was reduced in *Pik3r1*^{WT/Y657*} mice (**Figures 3I-L and**

4   **S5A-D)**. As muscle insulin sensitivity was previously reported not to be reduced in

5   *Pik3r1*^{WT/R649W} mice [31], insulin responsiveness of soleus and extensor digitorum

6   longus (EDL) muscles was assessed *ex vivo*. Soleus and EDL muscle from

7   *Pik3r1*^{WT/Y657*} mice both showed a 1.3-fold reduction in insulin-stimulated

8   deoxyglucose uptake compared to wild-type muscle (**Figure 3M**). Insulin-induced

9   Akt phosphorylation was also markedly reduced in both types of muscle *ex vivo* to a

10   much more significant degree than *in vivo* (**Figures 3N,O** and **S5E**). This finding of

11   muscle insulin resistance using several different techniques, although at odds with

12   clamp studies reported previously, is consistent with the robust expression of *Pik3r1*

13   gene products in skeletal muscle.

14

15   **3.4 *Pik3r1*^{WT/Y657*} mice are hypolipidemic**

16   Having shown that, as in SHORT syndrome, heterozygous *Pik3r1*^{WT/Y657*} mice

17   show severe IR and reduced adiposity, we assessed whether, like humans, they do

18   not exhibit fatty liver nor metabolic dyslipidemia. In fed and fasting states, on either

19   chow or high fat diets, *Pik3r1*^{WT/Y657*} mice showed hypolipidemia, with lower plasma

20   total cholesterol and HDL cholesterol (**Table 1**). This was most striking in fed mice

21   on high fat diet, mirroring the lower glucose seen in *Pik3r1*^{WT/Y657*} mice in this state.

22   Plasma triglyceride concentration was also lower in heterozygous animals in all

23   states except when fasting state after HFD, and plasma free fatty acid concentration

24   was lower in all states except in fed animals maintained on chow. Similar

25   hypolipidemia was seen in chow-fed female mice on fasting (**Table S1**). No

26   difference was seen in VLDL concentrations in chow- or high fat-fed mice (**Table 1**).

27   Despite severe IR in *Pik3r1*^{WT/Y657*} mice, no difference was seen in liver

28   triglyceride content compared to controls either on chow or HFD, assessed by Oil-

1   Red-O staining and biochemical quantification (**Figure 4A,B**). Liver cholesterol

2   content was also the same in chow-fed animals of both genotypes (**Figure 4C**). Oral

3   lipid tolerance testing revealed similar triglyceride excursion after lipid loading in both

4   genotypes (**Figure 4D**), and bomb calorimetry of feces on chow showed the same

5   energy content (**Figure 4E**), excluding abnormal intestinal lipid handling as the

6   explanation for hypolipidemia and reduced adiposity.

7   Insulin stimulates hepatic *de novo* lipogenesis and cholesterogenesis *via*

8   *Srebp1* and *Srebp2* respectively. In prevalent IR, hepatic *de novo* lipogenesis is

9   enhanced, and the mismatch between this and the reduced hypoglycemic action of

10   insulin is evidence for "partial IR" in metabolic dyslipidemia [19].   Liver PI3K

11   mediates the action of insulin on lipogenesis, with hypolipidemia despite IR seen in

12   numerous models in which hepatic insulin/Irs/PI3K/Akt2/mTORC2 signaling is

13   impaired [14–16,18,32]. Based on these findings, we hypothesised that the

14   hypolipidemia seen in *Pik3r1$^{Y657*/WT}$* mice would be accounted for by reduced hepatic

15   *de novo* lipogenesis, as in SHORT syndrome due to PIK3R1 Y657*[7]. In keeping

16   with this, no increased *de novo* synthesis of palmitate could be measured in

17   heterozygotes despite fasting hyperinsulinemia and refeeding with a high

18   carbohydrate diet (**Figure 4F**). Liver mRNA expression of *Srebp1c*, *Srebp2* and key

19   target genes (*Acc1*, *Fasn*, *Scd1 and Mvk*, *Nsdhl, respectively*) was also determined

20   in chow-fed animals in fed, fasting and refed states, and no difference was seen in

21   expression of any of these genes under any nutritional conditions (**Figure 4G-M**).

22   Other transcriptional regulators relevant to hypolipidemia include carbohydrate

23   response element binding protein (*Chrebp*) and *Xbp1*, with the latter binding p85α

24   and facilitating its nuclear translocation [31,33,34] A sentinel *Chrebp*-responsive

25   gene (*Pklr*) showed mild but significant reduction of mRNA in the fasting state, but

26   mRNA of two *Xbp1* target genes (*Acacb* and *Dgat2*) showed no reduction during a

27   fasting refeeding cycle (**Figure S6A-C**). It has also been proposed that modulation

28   of the ratio between Glucose-6-phosphatase (*G6pc*) and Glucokinase (*Gck*) toggles

1 hepatocyte glucose flux between lipogenesis and glucose production, and that this

2 operates before transcriptional changes in lipogenic transcription factors [35].

3 However, although an increase in *G6pc:Gck* liver transcript levels was seen on

4 fasting of wild-type mice, the ratio was suppressed in *Pik3r1*^{*WT/Y657**} mice, as reported

5 in mice on Western-type diet [35] (**Figure S6D-F**). We conclude that the consistent

6 hypolipidemia seen in *Pik3r1*^{*WT/Y657**} mice does not correlate with attenuated insulin-

7 induced lipogenesis in the liver, suggesting that the reduced blood lipid

8 concentrations are not explained by attenuation of insulin's lipogenic actions.

9 Given lack of transcriptional perturbation of known lipogenic factors, global

10 liver transcriptomic analysis was undertaken in fed and 16 hour fasted states.

11 Genotypes were compared in each state, and fasting gene expression was

12 compared to fed gene expression for both genotypes. Gene-based analysis

13 confirmed prior findings, but provided no obvious alternative explanation for

14 hypolipidemia. Pathway analysis of predicted upstream regulators showed modest

15 but significant differences in the fed state, with a transcriptional signature of reduced

16 ER stress (upstream regulators *Xbp1*, its processing enzyme *Ern1* (*Ire1*), and *Atf6*),

17 and altered signatures of several cytokines including *IL6* (reduced), *IL21*, interferons

18 gamma and alpha 2 (increased)(**Figure 5**, **Table S2**). More significant differences

19 were seen after 16-hour fasting, when a transcriptional profile consistent with

20 reduced activity of *Rictor*, the defining component of mTORC2, was seen with high

21 significance, while patterns associated with *Myc* and *Mycn* were upregulated. The

22 large preponderance of changes observed between fed and fasting states in wild

23 type mice, including strong upregulation of PPARα-responsive genes, was

24 conserved in heterozygous animals, however (**Figure 5**, **Table S2**).

25 In view of transcriptomic evidence of reduced Rictor activity, plasma and

26 hepatic amino acid and β-hydroxybutyrate concentrations were determined. This

27 revealed increased β-hydroxybutyrate in liver from fed *Pik3r1*^{*WT/Y657**} mice with a

1   trend towards an increase in plasma, but no difference between genotypes when

2   fasted (**Figure S7A**). The fall in plasma amino acid concentrations seen in fasting

3   wildtype mice was lost in *Pik3r1*$^{WT/Y657*}$ mice, with a trend towards a generalised

4   increase in liver amino acids (**Figure S7B,C**). These findings add to evidence for

5   abnormal transitions between fed and fasted state in *Pik3r1*$^{WT/Y657*}$ mice, and suggest

6   that reduced intra-hepatocyte amino acid concentrations on fasting do not explain

7   the pronounced reduction in Rictor signaling suggested by transcriptomics.

8

9   **4. Discussion**

10   Most monogenic defects causing severe IR primarily affect adipose tissue

11   development, and metabolically phenocopy common IR [1]. In contrast, humans

12   with severe IR due to proximal insulin signalling defects do not have the

13   dyslipidemia, fatty liver, and decreased plasma adiponectin concentration usual in

14   common IR [6,7,13,36]. This was first noted in people with insulin receptor

15   mutations [13], but more recently was described in SHORT syndrome, [6,7], in which

16   lack of fatty liver and dyslipidemia is particularly striking given concomitant

17   lipodystrophy. Fatty liver and atherogenic dyslipidemia are major sources of IR-

18   related morbidity, so investigating how these are dissociated from IR in the face of

19   proximal insulin signaling defects will potentially reveal novel approaches to mitigate

20   IR-associated disease.

21   The novel mice generated, heterozygous for the Pik3r1 Y657* allele, show

22   reduced growth, severe IR, and severely reduced adipose accretion on high fat

23   feeding. Although IR in *Pik3r1*$^{R649W/WT}$ mice described previously was reported to

24   spare skeletal muscle[31], we found skeletal muscle to be insulin resistant both in

25   clamps, and *ex vivo,* in keeping with ubiquitous expression of the mutant allele.

26   Despite severe IR, *Pik3r1*$^{WT/Y657*}$ mice were hypolipidemic on chow or high fat

27   diet, and in fed and fasted states, while the increase in liver triglyceride usual in

28   lipodystrophic IR was absent, validating it as a model of the human phenomenon we

15

1   aimed to study.   Knockout evidence that PI3K signaling mediates insulin's

2   stimulation of liver *de novo* lipogenesis led us to expect reduced transcript levels of

3   *Srebp* and its target genes (e.g. [16],[17]), however we found no evidence supporting

4   this or other candidate transcriptional mechanisms including reduced lipogenic

5   activity of *Xbp1* [34].

6   RNA sequencing showed most insulin-responsive genes to respond normally

7   to fasting and refeeding. Given elevated plasma insulin concentration this could be

8   construed as showing compensated hepatic IR, as expected from a proximal insulin

9   signaling defect. Fasting-responsive programmes, such as those orchestrated by

10 PPARα, were intact in *Pik3r1$^{Y657*/WT}$* mice, however pathway analysis suggested

11 reduced ER stress signaling and showed altered inflammatory signatures in the fed

12 state, with a strikingly reduced Rictor signature in the fasted state.   These

13 transcriptional clues may be pertinent to protection from dyslipidemia as ER stress

14 signaling promotes fatty liver and dyslipidemia [37], while Rictor drives hepatic

15 lipogenesis [38], however further study is needed. Impaired induction of Rictor

16 activity in this case may reflect Pik3r1's role in amino acid activation of Rictor [39].

17   *Pik3r1$^{R649W/WT}$* mice have been shown to have less subcutaneous adipose

18 tissue [31] and reduced adipose expansion in obesogenic conditions [40], as in the

19 current report, which was interpreted as evidence of lipodystrophy.   However

20 constrained adipose expansion produces inflammation of overloaded, hypertrophic

21 adipose tissue during chronic positive energy balance [1], and the normal adipocyte

22 appearance, lack of adipose inflammation, and normal differentiation of

23 preadipocytes *ex vivo* in both studies argues against this [31].

24   Reduced adipose mass can reflect altered energy balance rather than

25 lipodystrophy. Reduction of PI3K pathway activity by overexpression of the lipid

26 phosphatase *Pten* in mice was previously reported to enhance energy expenditure

27 via brown adipose tissue activation [41], albeit without IR, while pharmacological or

genetic inhibition of the p110α catalytic subunit of PI3K has also been associated

with increased energy expenditure [40–43]. Moreover a similar energetic phenotype

has recently been described on brown adipose-specific knockout of Pik3r1 [44]. On

high fat diet we found food intake and energy expenditure were both increased in

$Pik3r1^{Y657*/WT}$ mice. Given unaltered locomotor activity, intestinal lipid absorption,

and lean tissue growth, reduced adipose accumulation shows that increased energy

expenditure outweighed increased food intake, and is thus the primary abnormality.

Reduced thermal insulation in smaller animals is an unlikely explanation [43], so we

conclude that increased energy expenditure explains reduced adipose accretion.

Increased brown adipose tissue activity is the most likely explanation, as in models

with p110α inhibition[40–43], but this requires further study.

Increasing brown adipose tissue function reduces plasma triglyceride and

cholesterol concentrations[45,46], and this reduces atherogenesis when liver

scavenging of triglyceride-depleted lipoproteins is intact [45]. This accords with the

hypolipidemia of $Pik3r1^{Y657*/WT}$ mice, and also humans with SHORT syndrome. As

brown fat is now known to occur in humans, it would be of interest to establish

whether it is hyperactive in people with SHORT syndrome. In addition, given the

normal lipid profile despite severe IR in people with insulin receptor mutations [13],

and the reduced adipose tissue in mice harbouring a common dominant negative

insulin receptor allele on an obesogenic diet [47], it will be of interest to assess

whether the bioenergetic consequences of reduced PI3K signaling are also seen in

the face of insulin receptor dysfunction.

5. Conclusions

We report a novel mouse model of SHORT syndrome recapitulating the severe

IR without dyslipidemia seen in humans. Hepatic lipogenesis and lipogenic gene

expression were unimpaired, and transcriptomic pathway analysis suggested only

mild nutritional state-specific abnormalities in liver gene expression. White adipose

1 tissue was reduced on high fat diet, but did not show inflammation of hypertrophy,

2 while energy expenditure was increased, raising the testable possibility that the

3 reduced adipose mass in SHORT syndrome does not represent true "lipodystrophy".

4 The most likely mechanism explaining uncoupling of IR from dyslipidemia in SHORT

5 syndrome is increased brown adipose activity, consistent with other murine evidence

6 that inhibition of PI3K results in beneficial metabolic alterations as well as IR.

7

3   **Conflict of Interest**

4   The authors declare no conflicts of interest.

5   **6.   References**

6   [1]   Mann, J.P., Savage, D.B., 2019. What lipodystrophies teach us about the
7   metabolic syndrome. Journal of Clinical Investigation 130, Doi:
8   10.1172/jci129190.
9   [2]   Leiter, S.M., Semple, R.K., 2017. Insulin resistance and diabetes associated
10   with lipodystrophies. Diabetes Associated with Single Gene Defects and
11   Chromosomal Abnormalities, vol. 25. p. 119–33.
12 [3]   Chudasama, K.K., Winnay, J., Johansson, S., Claudi, T., König, R.,
13   Haldorsen, I., et al., 2013. SHORT syndrome with partial lipodystrophy due to
14   impaired phosphatidylinositol 3 kinase signaling. American Journal of Human
15   Genetics 93(1): 150–7, Doi: 10.1016/j.ajhg.2013.05.023.
16 [4]   Dyment, D.A., Smith, A.C., Alcantara, D., Schwartzentruber, J.A., Basel-
17   Vanagaite, L., Curry, C.J., et al., 2013. Mutations in PIK3R1 cause SHORT
18   syndrome. American Journal of Human Genetics 93(1): 158–66, Doi:
19   10.1016/j.ajhg.2013.06.005.
20 [5]   Thauvin-Robinet, C., Auclair, M., Duplomb, L., Caron-Debarle, M., Avila, M.,
21   St-Onge, J., et al., 2013. PIK3R1 mutations cause syndromic insulin
22   resistance with lipoatrophy. American Journal of Human Genetics 93(1): 141–
23   9, Doi: 10.1016/j.ajhg.2013.05.019.
24 [6]   Avila, M., Dyment, D.A., Sagen, J. V., St-Onge, J., Moog, U., Chung, B.H.Y.,
25   et al., 2016. Clinical reappraisal of SHORT syndrome with PIK3R1 mutations:
26   Toward recommendation for molecular testing and management. Clinical
27   Genetics 89(4): 501–6, Doi: 10.1111/cge.12688.
28 [7]   Huang-Doran, I., Tomlinson, P., Payne, F., Gast, A., Sleigh, A., Bottomley,
29   W., et al., 2016. Insulin resistance uncoupled from dyslipidemia due to C-
30   terminal PIK3R1 mutations. JCI Insight 1(17): e88766, Doi:
31   10.1172/jci.insight.88766.
32 [8]   Vanhaesebroeck, B., Stephens, L., Hawkins, P., 2012. PI3K signalling: the
33   path to discovery and understanding. Nature Reviews Molecular Cell Biology
34   13(3): 195–203, Doi: 10.1038/nrm3290.
35 [9]   Cantley, L.C., 2002. The Phosphoinositide 3-Kinase Pathway. Science
36   296(5573): 1655–7, Doi: 10.1126/science.296.5573.1655.
37 [10] Terauchi, Y., Tsuji, Y., Satoh, S., Minoura, H., Murakami, K., Okuno, a., et al.,
38   1999. Increased insulin sensitivity and hypoglycaemia in mice lacking the p85
39   alpha subunit of phosphoinositide 3-kinase. Nature Genetics 21(2): 230–5,
40   Doi: 10.1038/6023.
41 [11] Mauvais-Jarvis, F., Ueki, K., Fruman, D.A., Hirshman, M.F., Sakamoto, K.,
42   Goodyear, L.J., et al., 2002. Reduced expression of the murine p85alpha
43   subunit of phosphoinositide 3-kinase improves insulin signaling and
44   ameliorates diabetes. The Journal of Clinical Investigation 109(1): 141–9, Doi:
45   10.1172/JCI13305.
46 [12] Chen, D., Mauvais-Jarvis, F., Bluher, M., Fisher, S.J., Jozsi, A., Goodyear,
47   L.J., et al., 2004. p50 /p55 Phosphoinositide 3-Kinase Knockout Mice Exhibit
48   Enhanced Insulin Sensitivity. Molecular and Cellular Biology 24(1): 320–9,
49   Doi: 10.1128/MCB.24.1.320-329.2004.
50 [13] Semple, R.K., Sleigh, A., Murgatroyd, P.R., Adams, C.A., Bluck, L., Jackson,

1   S., et al., 2009. Postreceptor insulin resistance contributes to human
2   dyslipidemia and hepatic steatosis. Journal of Clinical Investigation 119(2):
3   315–22, Doi: 10.1172/JCI37432.

[14] Biddinger, S.B., Hernandez-Ono, A., Rask-Madsen, C., Haas, J.T., Alemán, J.O., Suzuki, R., et al., 2008. Hepatic Insulin Resistance Is Sufficient to Produce Dyslipidemia and Susceptibility to Atherosclerosis. Cell Metabolism 7(2): 125–34, Doi: 10.1016/j.cmet.2007.11.013.

[15] Kubota, N., Kubota, T., Itoh, S., Kumagai, H., Kozono, H., Takamoto, I., et al., 2008. Dynamic Functional Relay between Insulin Receptor Substrate 1 and 2 in Hepatic Insulin Signaling during Fasting and Feeding. Cell Metabolism 8(1): 49–64, Doi: 10.1016/j.cmet.2008.05.007.

[16] Taniguchi, C.M., Kondo, T., Sajan, M., Luo, J., Bronson, R., Asano, T., et al., 2006. Divergent regulation of hepatic glucose and lipid metabolism by phosphoinositide 3-kinase via Akt and PKCλ/ζ. Cell Metabolism 3(5): 343–53, Doi: 10.1016/j.cmet.2006.04.005.

[17] Sopasakis, V.R., Liu, P., Suzuki, R., Kondo, T., Winnay, J., Tran, T.T., et al., 2010. Specific Roles of the p110α Isoform of Phosphatidylinsositol 3-Kinase in Hepatic Insulin Signaling and Metabolic Regulation. Cell Metabolism 11(3): 220–30, Doi: 10.1016/j.cmet.2010.02.002.

[18] Hagiwara, A., Cornu, M., Cybulski, N., Polak, P., Betz, C., Trapani, F., et al., 2012. Hepatic mTORC2 activates glycolysis and lipogenesis through Akt, glucokinase, and SREBP1c. Cell Metabolism 15(5): 725–38, Doi: 10.1016/j.cmet.2012.03.015.

[19] Brown, M.S., Goldstein, J.L., 2008. Selective versus Total Insulin Resistance: A Pathogenic Paradox. Cell Metabolism: 95–6, Doi: 10.1016/j.cmet.2007.12.009.

[20] Whittle, A.J., Jiang, M., Peirce, V., Relat, J., Virtue, S., Ebinuma, H., et al., 2015. Soluble LR11/SorLA represses thermogenesis in adipose tissue and correlates with BMI in humans. Nature Communications 6: 8951, Doi: 10.1038/ncomms9951.

[21] Schreiber, R., Hofer, P., Taschler, U., Voshol, P.J., Rechberger, G.N., Kotzbeck, P., et al., 2015. Hypophagia and metabolic adaptations in mice with defective ATGL-mediated lipolysis cause resistance to HFD-induced obesity. Proceedings of the National Academy of Sciences of the United States of America 112(45): 13850–5, Doi: 10.1073/pnas.1516004112.

[22] Sell, H., Jensen, J., Eckel, J., 2012. Measurement of Insulin Sensitivity in Skeletal Muscle In Vitro. Methods Mol Biol 933: 255–63, Doi: 10.1007/978-1-62703-068-7.

[23] Lowry, O.H., Passonneau, J. V., 1972. A flexible system of enzyme analysis. Academic Press.

[24] Horscroft, J.A., Kotwica, A.O., Laner, V., West, J.A., Hennis, P.J., Levett, D.Z.H., et al., 2017. Metabolic basis to Sherpa altitude adaptation. Proceedings of the National Academy of Sciences 114(24): 6382–7, Doi: 10.1073/pnas.1700527114.

[25] Roberts, L.D., Virtue, S., Vidal-Puig, A., Nicholls, A.W., Griffin, J.L., Bethell, D., et al., 2009. Metabolic phenotyping of a model of adipocyte differentiation. Physiological Genomics 39(2): 109–19, Doi: 10.1152/physiolgenomics.90365.2008.

[26] Virtue, S., Feldmann, H., Christian, M., Tan, C.Y., Masoodi, M., Dale, M., et al., 2012. A new role for lipocalin prostaglandin D synthase in the regulation of brown adipose tissue substrate utilization. Diabetes 61(12): 3139–47, Doi: 10.2337/db12-0015.

[27] Mauro, C., Smith, J., Cucchi, D., Coe, D., Fu, H., Bonacina, F., et al., 2017. Obesity-Induced Metabolic Stress Leads to Biased Effector Memory CD4+ T Cell Differentiation via PI3K p110δ-Akt-Mediated Signals. Cell Metabolism

1   25(3): 593–609, Doi: 10.1016/j.cmet.2017.01.008.

2   [28] Larder, R., Sim, M.F.M., Gulati, P., Antrobus, R., Tung, Y.C.L., Rimmington,
3   D., et al., 2017. Obesity-associated gene TMEM18 has a role in the central
4   control of appetite and body weight regulation. Proceedings of the National
5   Academy of Sciences 114(35): 9421–6, Doi: 10.1073/pnas.1707310114.

6   [29] Rocha, N., Bulger, D.A., Frontini, A., Titheradge, H., Gribsholt, S.B., Knox, R.,
7   et al., 2017. Human biallelic MFN2 mutations induce mitochondrial
8   dysfunction, upper body adipose hyperplasia, and suppression of leptin
9   expression. ELife 6, Doi: 10.7554/elife.23813.

10 [30] Ko, H.R., Kim, C.K., Lee, S.B., Song, J., Lee, K.-H., Kim, K.K., et al., 2014.
11   P42 Ebp1 regulates the proteasomal degradation of the p85 regulatory
12   subunit of PI3K by recruiting a chaperone-E3 ligase complex HSP70/CHIP.
13   Cell Death & Disease 5(3): e1131, Doi: 10.1038/cddis.2014.79.

14 [31] Winnay, J.N., Solheim, M.H., Dirice, E., Sakaguchi, M., Noh, H.L., Kang, H.J.,
15   et al., 2016. PI3-kinase mutation linked to insulin and growth factor resistance
16   in vivo. Journal of Clinical Investigation 126(4): 1401–12, Doi:
17   10.1172/JCI84005.

18 [32] Leavens, K.F., Easton, R.M., Shulman, G.I., Previs, S.F., Birnbaum, M.J.,
19   2009. Akt2 Is Required for Hepatic Lipid Accumulation in Models of Insulin
20   Resistance. Cell Metabolism 10(5): 405–18, Doi: 10.1016/j.cmet.2009.10.004.

21 [33] Park, S.W., Zhou, Y., Lee, J., Lu, A., Sun, C., Chung, J., et al., 2010. The
22   regulatory subunits of PI3K, p85α and p85β, interact with XBP-1 and increase
23   its nuclear translocation. Nature Medicine 16(4): 429–37, Doi:
24   10.1038/nm.2099.

25 [34] Lee, A.-H., Scapa, E.F., Cohen, D.E., Glimcher, L.H., 2008. Regulation of
26   Hepatic Lipogenesis by the Transcription Factor XBP1. Science 320(5882):
27   1492–6, Doi: 10.1126/science.1158042.

28 [35] Haeusler, R.A., Hartil, K., Vaitheesvaran, B., Arrieta-Cruz, I., Knight, C.M.,
29   Cook, J.R., et al., 2014. Integrated control of hepatic lipogenesis versus
30   glucose production requires FoxO transcription factors. Nature
31   Communications 5: 5190, Doi: 10.1038/ncomms6190.

32 [36] Semple, R.K., Soos, M.A., Luan, J., Mitchell, C.S., Wilson, J.C., Gurnell, M., et
33   al., 2006. Elevated plasma adiponectin in humans with genetically defective
34   insulin receptors. Journal of Clinical Endocrinology and Metabolism 91(8):
35   3219–23, Doi: 10.1210/jc.2006-0166.

36 [37] Wang, L., Chen, J., Ning, C., Lei, D., Ren, J., 2018. Endoplasmic reticulum
37   stress related molecular mechanisms in nonalcoholic fatty liver disease
38   (NAFLD). Current Drug Targets 19, Doi:
39   10.2174/1389450118666180516122517.

40 [38] Yuan, M., Pino, E., Wu, L., Kacergis, M., Soukas, A.A., 2012. Identification of
41   Akt-independent regulation of hepatic lipogenesis by mammalian target of
42   rapamycin (mTOR) complex 2. The Journal of Biological Chemistry 287(35):
43   29579–88, Doi: 10.1074/jbc.M112.386854.

44 [39] Tato, I., Bartrons, R., Ventura, F., Rosa, J.L., 2011. Amino acids activate
45   mammalian target of rapamycin complex 2 (mTORC2) via PI3K/Akt signaling.
46   The Journal of Biological Chemistry 286(8): 6128–42, Doi:
47   10.1074/jbc.M110.166991.

48 [40] Solheim, M.H., Winnay, J.N., Batista, T.M., Molven, A., Njølstad, P.R., Kahn,
49   C.R., 2018. Mice Carrying a Dominant-Negative Human PI 3-Kinase Mutation
50   are Protected From Obesity and Hepatic Steatosis But Not Diabetes. Diabetes
51   67(7): db171509, Doi: 10.2337/db17-1509.

52 [41] Ortega-Molina, A., Efeyan, A., Lopez-Guadamillas, E., Muñoz-Martin, M.,
53   Gómez-López, G., Cañamero, M., et al., 2012. Pten positively regulates
54   brown adipose function, energy expenditure, and longevity. Cell Metabolism
55   15(3): 382–94, Doi: 10.1016/j.cmet.2012.02.001.

1   [42]   Araiz, C., Yan, A., Bettedi, L., Samuelson, I., Virtue, S., McGavigan, A.K., et
2   al., 2019. Enhanced β-adrenergic signalling underlies an age-dependent
3   beneficial metabolic effect of PI3K p110α inactivation in adipose tissue.
4   Nature Communications in press(1): 1546, Doi: 10.1038/s41467-019-09514-1.
5   [43]   Fischer, A.W., Csikasz, R.I., von Essen, G., Cannon, B., Nedergaard, J.,
6   2016. No insulating effect of obesity. American Journal of Physiology -
7   Endocrinology And Metabolism 311(1): E202–13, Doi:
8   10.1152/ajpendo.00093.2016.
9   [44]   Gomez-Hernandez, A., Lopez-Pastor, A.R., Rubio-Longas, C., Majewski, P.,
10   Beneit, N., Viana-Huete, V., et al., 2020. Specific knockout of p85α in brown
11   adipose tissue induces resistance to high-fat diet–induced obesity and its
12   metabolic complications in male mice. Molecular Metabolism 31: 1–13, Doi:
13   10.1016/j.molmet.2019.10.010.
14   [45]   Berbeé, J.F.P., Boon, M.R., Khedoe, P.P.S.J., Bartelt, A., Schlein, C.,
15   Worthmann, A., et al., 2015. Brown fat activation reduces
16   hypercholesterolaemia and protects from atherosclerosis development.
17   Nature Communications 6: 6356, Doi: 10.1038/ncomms7356.
18   [46]   Dong, M., Yang, X., Lim, S., Cao, Z., Honek, J., Lu, H., et al., 2013. Cold
19   exposure promotes atherosclerotic plaque growth and instability via UCP1-
20   dependent lipolysis. Cell Metabolism 18(1): 118–29, Doi:
21   10.1016/j.cmet.2013.06.003.
22   [47]   Lee, E.Y., Sakurai, K., Zhang, X., Toda, C., Tanaka, T., Jiang, M., et al., 2015.
23   Unsuppressed lipolysis in adipocytes is linked with enhanced
24   gluconeogenesis and altered bile acid physiology in Insr(P1195L/+) mice fed
25   high-fat-diet. Scientific Reports 5: 17565, Doi: 10.1038/srep17565.
26
27

Tables

	Chow						45% Fat Diet					
	Fasting			Fed			Fasting			Fed		
	$Pik3r1^{WT/WT}$ (n=10)	$Pik3r1^{WT/Y657*}$ (n=9)	p	$Pik3r1^{WT/WT}$ (n=10)	$Pik3r1^{WT/Y657*}$ (n=14)	p	$Pik3r1^{WT/WT}$ (n=13)	$Pik3r1^{WT/Y657*}$ (n=13)	p	Pik3r1$^{WT/WT}$ (n=15)	Pik3r1$^{WT/Y657*}$ (n=11)	p
Glucose (mmol/L)	10.2 ± 1.1	9.0 ± 1.1	0.43	12.5 ± 0.7	13.2 ± 0.5	0.48	9.7 ± 0.8	7.9 ± 0.5	0.06	12.6 ± 0.5	9.4 ± 0.5	4×10^{-4}
Insulin (pmol/L)	138 ± 21	603 ± 202	0.05	229 ± 33	3393 ± 578	1.9×10^{-4}	469 ± 77	693 ± 102	0.09	424 ± 73	1313 ± 494	0.104
Adiponectin (mg/L)	30.5 ± 1.1	26.7 ± 1.3	0.03	33.2 ± 1.5	35.6 ± 1.0	0.2	37.0 ± 1.1	40.6 ± 1.5	0.07	40.3 ± 2.2	42.8 ± 1.1	0.3
Total cholesterol (mmol/L)	2.7 ± 0.1	2.3 ± 0.1	0.01	2.6 ± 0.1	2.0 ± 0.1	6×10^{-3}	4.2 ± 0.2	3.0 ± 0.3	0.01	4.7 ± 0.3	1.7 ± 0.1	1.0×10^{-7}
HDL cholesterol (mmol/L)	1.5 ± 0.1	1.1 ± 0.1	0.02	1.6 ± 0.1	1.3 ± 0.1	0.04	1.8 ± 0.2	1.2 ± 0.2	0.02	2.3 ± 0.1	0.9 ± 0.1	2.7×10^{-8}
Triglycerides (mmol/L)	1.5 ± 0.1	1.0 ± 0.1	0.01	1.6 ± 0.1	1.1 ± 0.1	0.01	1.5 ± 0.1	1.4 ± 0.1	0.15	1.0 ± 0.1	0.6 ± 0.02	3.5×10^{-6}
NEFA (mmol/L)	2.0 ± 0.2	1.2 ± 0.1	5×10^{-3}	1.5 ± 0.1	1.3 ± 0.2	0.3	2.5 ± 0.2	1.9 ± 0.1	0.05	1.5 ± 0.1	0.8 ± 0.1	7×10^{-5}
VLDL (mg/mL)	N.D.	N.D.	N.D.	7.9 ± 0.3	7.4 ± 1.2	0.25	N.D.	N.D.	N.D.	10.5 ± 0.5	11.9 ± 0.8	0.13

Table 1. Fasting plasma biochemical profile of male *Pik3r1$^{WT/WT}$* and *Pik3r1$^{WT/Y657*}$* mice. See also Supplemental Table S1 for fasting biochemical profile for chow-fed female mice. N.D. = not determined. Statistical comparisons were undertaken using the student's t-test.

23

Figure Legends

Figure 1. Effect of *Pik3r1* Y657* on prenatal development and postnatal growth.
(A) Representative image of *Pik3r1^{WT/WT}* (WT/WT) and *Pik3r1^{WT/Y657*}* (WT/Y657*) mice at 18 weeks old. (B) Body lengths (nose to anus) at 18 weeks of *Pik3r1^{WT/WT}* and *Pik3r1^{WT/Y657*}* mice (n=11 and 18 respectively). (C) Bodyweight increase from 8 to 16 weeks of *Pik3r1^{WT/WT}* and *Pik3r1^{WT/Y657*}* (n=16 and 12 respectively). (D) The relationship between lean and fat mass of *Pik3r1^{WT/WT}* and *Pik3r1^{WT/Y657*}* mice (n =16 and 12 respectively). Masses of (E) inguinal adipose tissue (IngWAT) (F) Epididymal adipose tissue (eWAT), (G) Brown adipose tissue (BAT), (H) Liver, and (I) Heart of *Pik3r1^{WT/WT}* and *Pik3r1^{WT/Y657*}* mice (n= 11 and 7 respectively). (J) Food intake (n=13 for *Pik3r1^{WT/WT}* and n=14 for *Pik3r1^{WT/Y657*}*), (K) Energy expenditure and (L) Respiratory exchange ratio (RER) (n=7 for *Pik3r1^{WT/WT}* and n=13 for *Pik3r1^{WT/Y657*}*) of wild type and heterozygous mice assessed at 18 weeks old. All data shown are from male mice. Masses and energy expenditure are shown relative to total lean mass, and were analysed statistically by ANCOVA. * = $p < 0.05$; *** = $p < 0.001$; **** = $p < 0.0001$. Mean ± SD are shown for plots in (B), (C) and (I).

Figure 2. Response of *Pik3r1^{WT/Y657*}* mice to a palatable 45% fat diet. (A) Bodyweight increase from 8 to 16 weeks of *Pik3r1^{WT/WT}* (WT/WT) and *Pik3r1^{WT/Y657*}* (WT/Y657*) (n=16 and 12 respectively). (B) The relationship between lean and fat mass of *Pik3r1^{WT/WT}* and *Pik3r1^{WT/Y657*}* mice (n =16 and 12 respectively). Masses of (C) Epididymal adipose tissue (eWAT), (D) Inguinal adipose tissue (IngWAT), (E) Brown adipose tissue (BAT), (F) Liver, and (G) Heart of *Pik3r1^{WT/WT}* and *Pik3r1^{WT/Y657*}* mice (n= 12 for both genotypes). (H) Representative histological appearance of haematoxylin and eosin-stained eWAT from *Pik3r1^{WT/WT}* and *Pik3r1^{WT/Y657*}* mice. Scale bars = 100μm (I) Adipocyte size distribution in eWAT based on quantification of >1,000 cells per genotype from 4 wild type and 4

heterozygous mice. The inset shows a zoomed-in view of the % of cells smaller than 10000μm^2. (J) Representative images of *ex vivo* differentiated stromal vascular cells from ingWAT stained with Oil Red O. (K) % of CD4$^+$ and regulatory T cells in the eWAT (n=3 for *Pik3r1$^{WT/WT}$* and n=3 for *Pik3r1$^{WT/Y657*}$*). (L) Food intake (n=13 for *Pik3r1$^{WT/WT}$* and n=14 for *Pik3r1$^{WT/Y657*}$*) and (M) Energy expenditure (n=17 for *Pik3r1$^{WT/WT}$* and n=10 for *Pik3r1$^{WT/Y657*}$*) of wild type and heterozygous mice assessed at 18 weeks old. All masses and energy expenditure are shown relative to total lean mass, and were analysed statistically by ANCOVA. (N) Locomotor activity of *Pik3r1$^{WT/WT}$* and *Pik3r1$^{WT/Y657*}$* mice (n=17 and n-10 respectively). (O) Respiratory exchange ratio (RER) (n=17 for *Pik3r1$^{WT/WT}$* and n=10 for *Pik3r1$^{WT/Y657*}$*) of wild type and heterozygous mice assessed at 18 weeks old. All data shown are from male mice. Mean ± SD are shown. *p < 0.05, **p < 0.01, ***p < 0.001 and ****p < 0.0001.

Figure 3. *Pik3r1$^{WT/Y657*}$* mice show systemic and tissue-level insulin resistance. (A) Glucose infusion rates during hyperinsulinemic euglycemic clamping of *Pik3r1$^{WT/WT}$* (WT/WT) and *Pik3r1$^{WT/Y657*}$* (WT/Y657*) mice on chow (n=4 and 4) or 45% fat diet (n=10 and 11) at 16 weeks old. (B) Oral glucose tolerance test (OGTT) and corresponding comparison of areas under the curves (AUC) of *Pik3r1$^{WT/WT}$* and *Pik3r1$^{WT/Y657*}$* mice on chow at 12 weeks old (n=10 and 9). (C) Insulin concentrations and AUC for the same OGTT as in (B). (D) Insulin tolerance test and AUC comparison for the same mice 1 week later. (E) Glucose disposal and (F) suppression of hepatic glucose output by insulin during hyperinsulinemic euglycemic clamping of *Pik3r1$^{WT/WT}$* and *Pik3r1$^{WT/Y657*}$* mice on chow at 18 weeks old (both n=4). (G) Glycogen content of livers during a fasting-refeeding cycle in chow fed animals at 16 weeks old (both n=6). (H) Plasma non-esterified free fatty acid concentrations during hyperinsulinemic euglycemic clamping (both genotypes n=4). (I)-(L) Representative images of immunoblots and corresponding quantifications of tissue lysates from mice injected intraperitoneally with 2U/kg insulin 10 mins prior to

25

sacrifice, showing pAkt^{Ser473}, total Akt and their ratio: (I) Liver, (J) Skeletal muscle (K) eWAT, (L) ingWAT. (n=6 per genotype and condition). (M) Insulin-induced fold increase of glucose uptake into *ex vivo* incubated soleus (n=18 for *Pik3r1$^{WT/WT}$*, n=11 for *Pik3r1$^{WT/Y657*}$*) and Extensor Digitorum Longus (EDL) (n=20 and 11). (N) Representative immunoblots of Soleus and EDL lysates from the same paradigm as in (M). (O) Quantification of pAkt^{Ser473} to total Akt ratios from soleus and EDL immunoblots (n=5 and 4 for both). Data are from male mice. Quantitative data are presented as mean ± SD. * = $p < 0.05$, ** = $p < 0.01$, *** = $p < 0.001$ and **** = $p < 0.0001$.

Figure 4. Lipid handling and liver phenotype of *Pik3r1$^{WT/Y657*}$* mice. (A) Representative images of Oil-Red-O-stained livers of chow-fed and 45% fat diet-fed *Pik3r1$^{WT/WT}$* (WT/WT) and *Pik3r1$^{WT/Y657*}$* (WT/Y657*) mice. Scale bars = 200μm. (B) Hepatic triglyceride and (C) Hepatic total cholesterol concentration during a fasting refeeding cycle of chow fed mice at 16 weeks old (n=6 per genotype). (D) Lipid tolerance testing and comparison of areas under the curve (AUC), also of chow-fed mice, at 16 weeks old. Triglyceride concentrations were equalised at baseline by matching the difference between genotypes with the lower values of heterozygous mice, and the same fixed correction was applied to all points on the graph (n = 11 and n=17 for wild-type and heterozygous mice respectively). (E) Faecal energy content determined by bomb calorimetry of chow fed mice at 16 weeks old (n=8 and 8). (F) De novo palmitate measured by stable deuterium enrichment (n=7 and n=10 for wild-type and heterozygous mice respectively). (G)-(M) Liver mRNA expression, determined by quantitative real time PCR of (G) *Srebp1* and its transcriptional targets (H) *Acc1*, (I) *Fasn*, and (J) *Scd1*, and of (K) *Srebp2* and its transcriptional targets (L) *Mvk* and (M) *Nsdhl* in chow fed mice during a fasting refeeding cycle at 16 weeks old (n=6 per genotype per condition). All data shown are from male mice. Numerical data are presented as mean ± SD.

Figure 5. Pathway analysis of liver transcriptomes of fed and fasted mice.
Volcano plots are shown for predicted upstream regulators derived from Ingenuity®
Pathway Analysis (IPA®) of transcriptomes of fed and fasted male $Pik3r1^{WT/Y657*}$
(n=6,6) mice and wildtype littermates (n=6,6). Outside plots show regulators showing
differential activity in the fasting state compared to the fed state for wildtype (WT;
left) and $Pik3r1^{WT/Y657*}$ (right) mice. Central plots show regulators with differential
activity in $Pik3r1^{WT/Y657*}$ vs WT mice in the fed state (top) and fasting state (bottom).
Green dots represent data point with an activation z score < -2 or > +2 and a p-value
< 1 x 10^{-5}. Regulators showing differential activity in either genotype-based
comparison are coloured red (activation z score > +2 in $Pik3r1^{WT/Y657*}$ vs WT mice)
or blue (activation z score < -2 in $Pik3r1^{WT/Y657*}$ vs WT mice) in the outside plots
showing differences based on nutritional state. Statistical analysis was performed
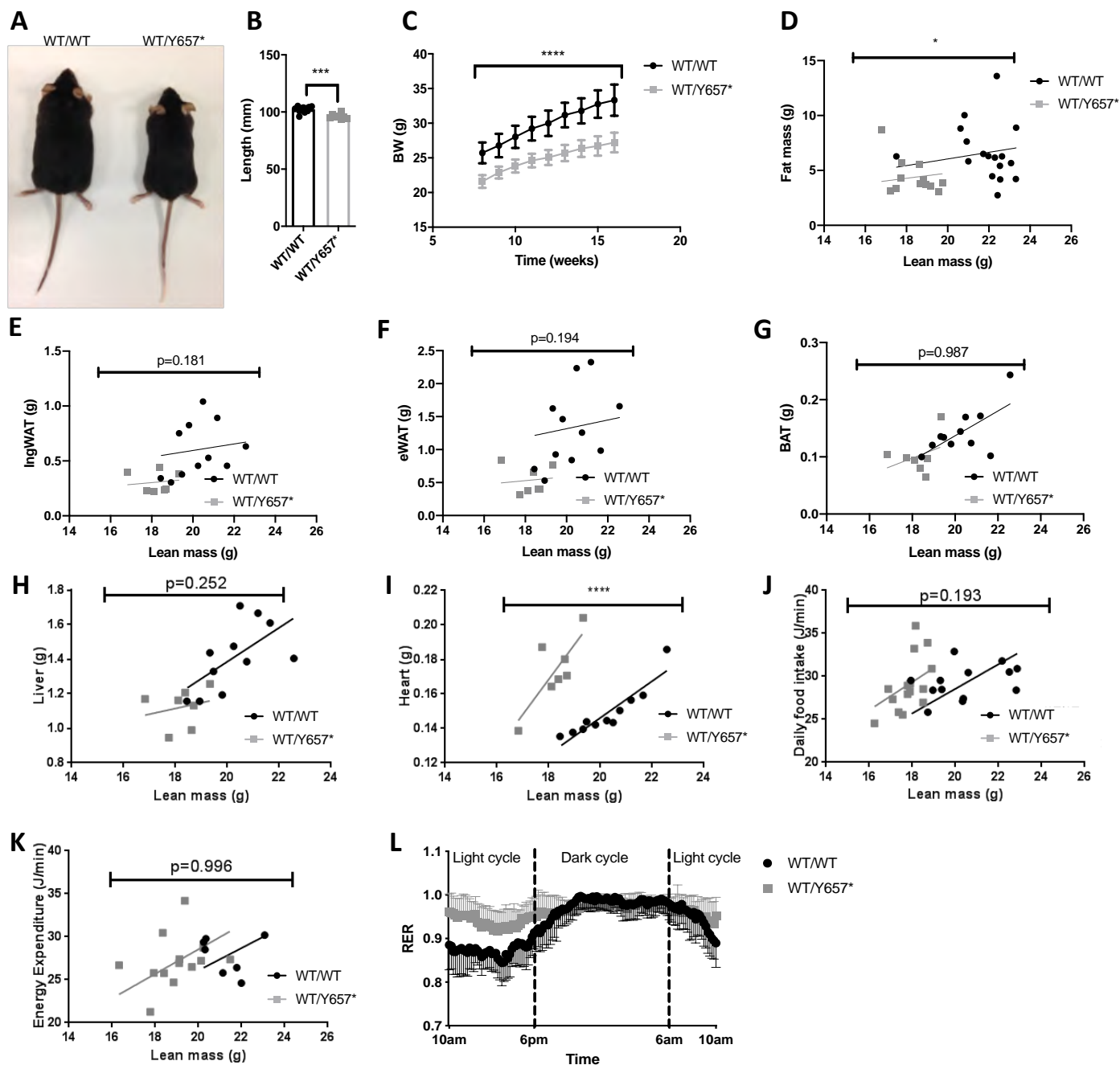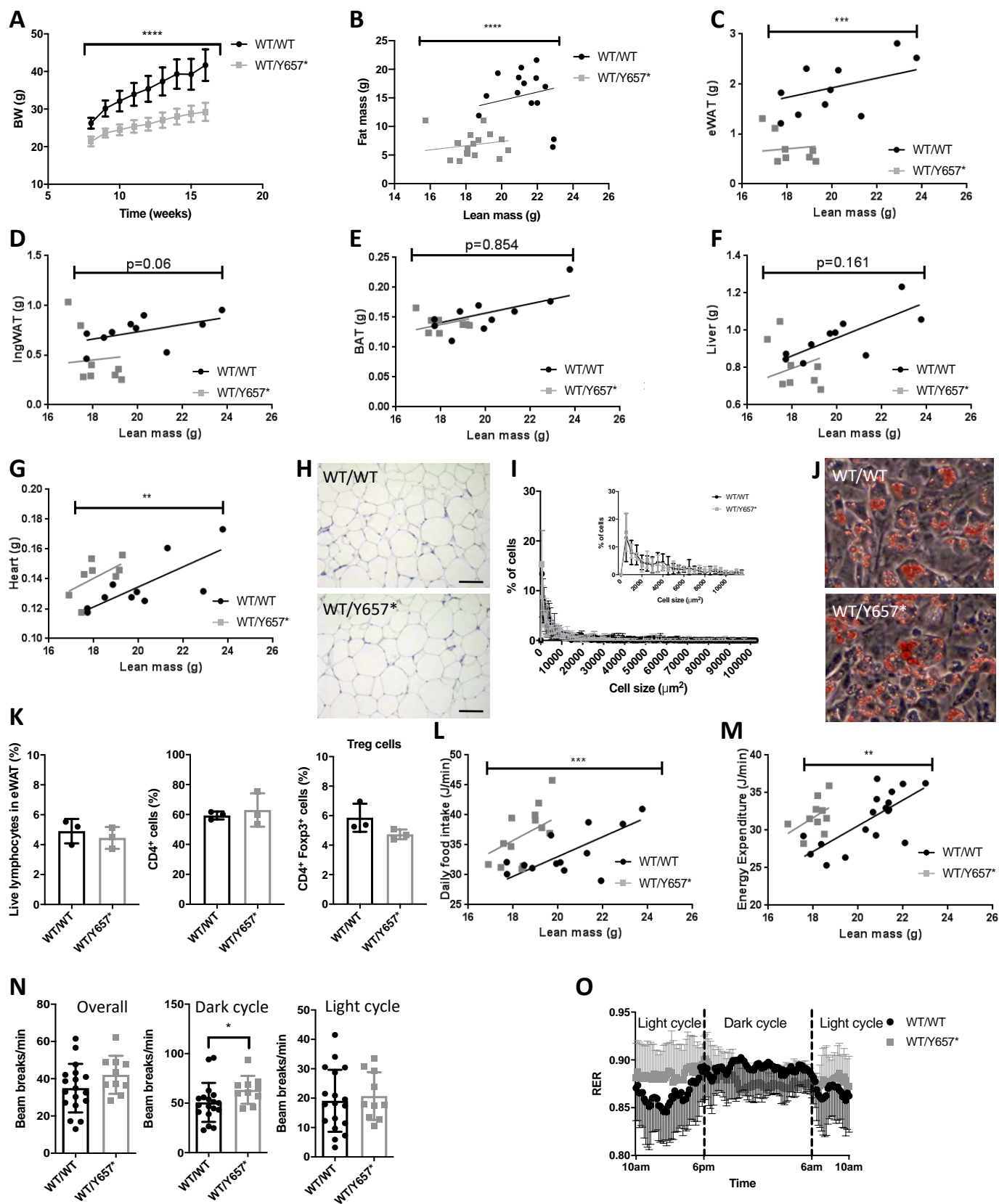using a general linear model with Bonferroni correction.
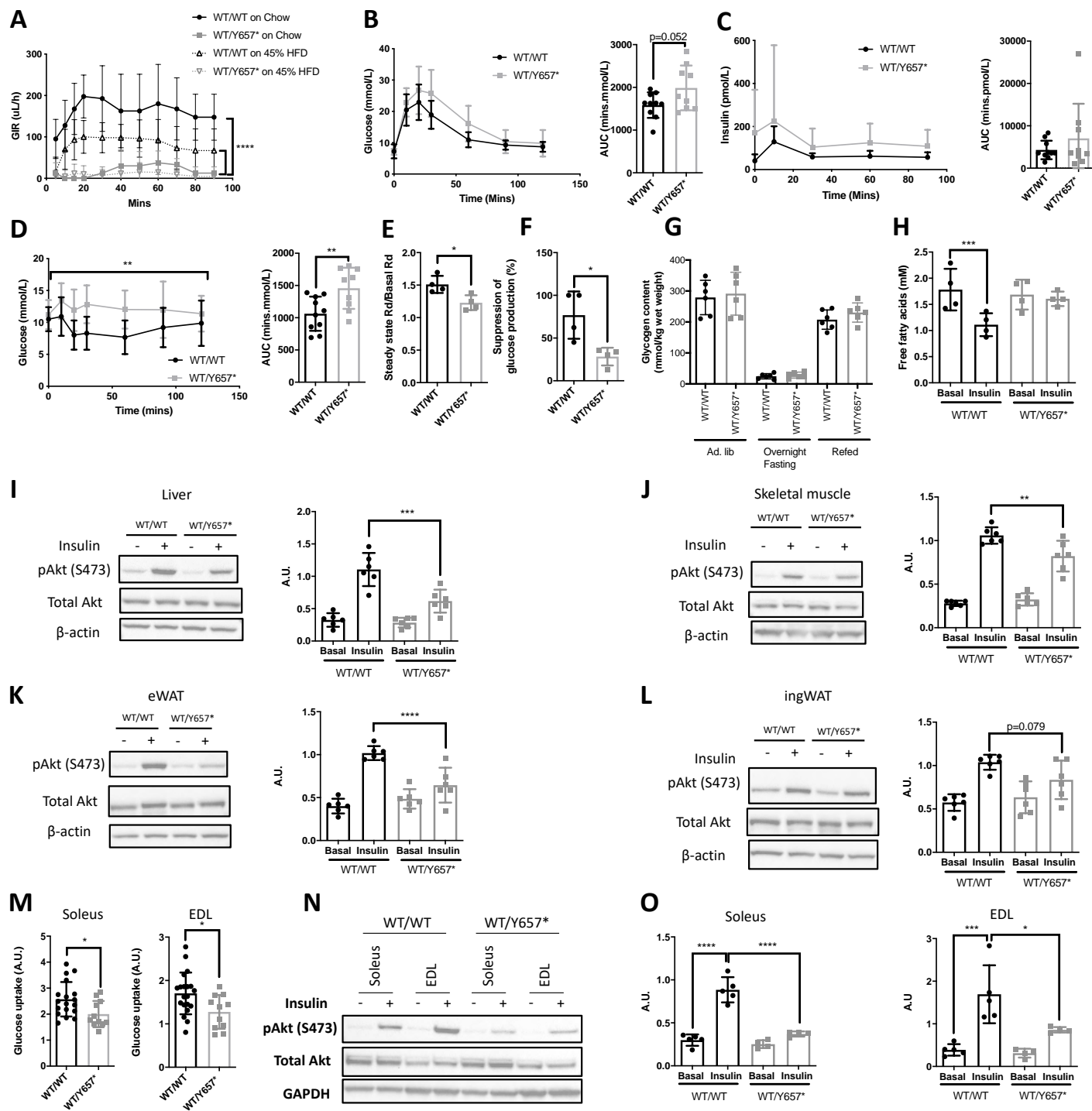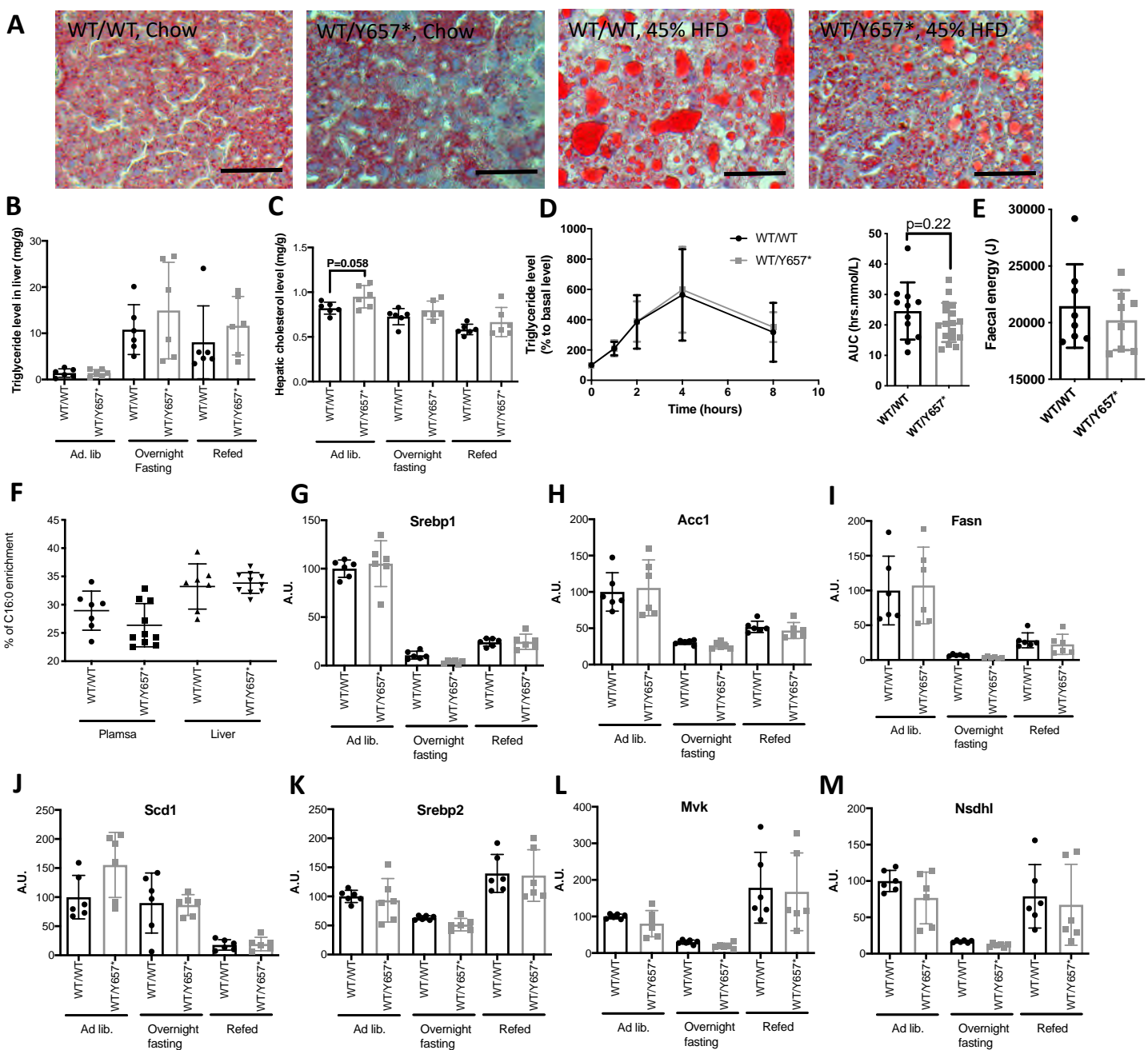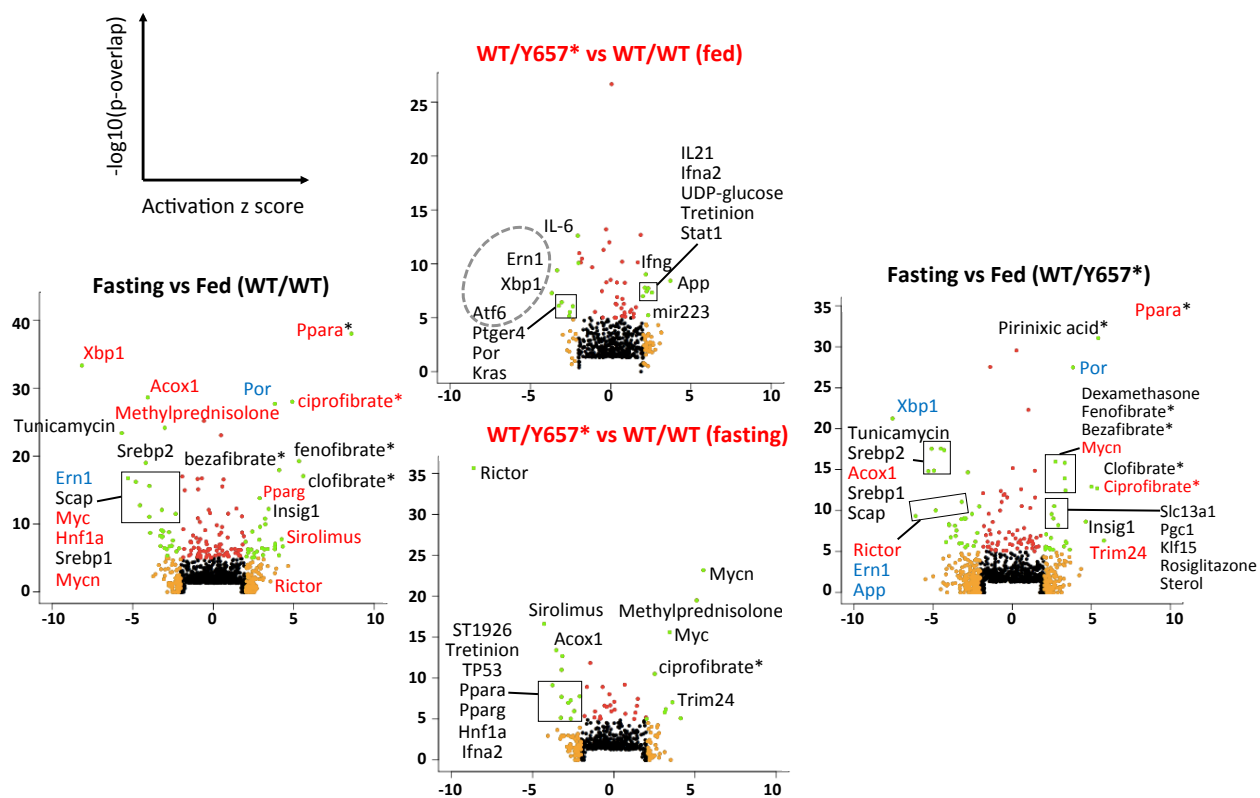
Fig. 1

Fig. 2

Fig. 3

Fig. 4

Fig. 5

Highlights

Truncation of Pik3r1 causes severe insulin resistance uncoupled from obesity and dyslipidemia by increased energy expenditure

Albert Kwok, Ilona Zvetkova, Sam Virtue, Ineke Luijten, Isabel Huang-Doran, Patsy Tomlinson, David A. Bulger, James West, Steven Murfitt, Julian Griffin, Rafeah Alam, Daniel Hart, Rachel Knox, Peter Voshol, Antonio Vidal-Puig, Jørgen Jensen, Stephen O'Rahilly, Robert K Semple

- Human SHORT syndrome includes severe insulin resistance and lipodystrophy

- Unlike other lipodystrophies, fatty liver and dyslipidaemia are not seen

- A mouse model with a pathogenic human PI 3-Kinase mutation recapitulates this uncoupling

- Surprisingly, no adipose injury nor increased liver de novo lipogenesis are seen

- Energy expenditure is increased, causing resistance to diet-induced obesity

- Reduced fat in humans with PI 3-Kinase dysfunction may not be true lipodystrophy

- This increases evidence for some beneficial metabolic effects of PI 3-Kinase inhibition

Conflicting interests Statement

Truncation of Pik3r1 causes severe insulin resistance uncoupled from obesity and dyslipidemia by increased energy expenditure

Albert Kwok, Ilona Zvetkova, Sam Virtue, Ineke Luijten, Isabel Huang-Doran, Patsy Tomlinson, David A. Bulger, James West, Steven Murfitt, Julian Griffin, Rafeah Alam, Daniel Hart, Rachel Knox, Peter Voshol, Antonio Vidal-Puig, Jørgen Jensen, Stephen O'Rahilly, Robert K Semple

Declarations of interest: none